

2.2 Control of Elementary Excitations by Acoustic Fields

This core research area aims at the use of acoustic waves as a tool for the manipulation of elementary excitations such as photons, electrons, spins, and excitons in semiconductor nanostructures. Most of the investigations are carried out using acoustic fields due to surface acoustic waves (SAWs) generated by interdigital transducers deposited on top of a piezoelectric substrate. The investigations cover the areas of acoustic transport of charge as well as spin and of acoustic modulation of microcavity polaritons.

Recently, we have demonstrated that SAWs can efficiently transport carriers in semiconductor nanostructures such as quantum wells and quantum wires. This field has matured to such an extent that it is now possible to exploit device concepts that take advantage of the unique features of acoustic transport. One of these concepts is the acousto-electric single-photon detector (ACDET). Here, electrons and holes excited through the absorption of the incoming photons are transported by a SAW to small charge collecting areas, where they are detected with single-charge sensitivity by radio-frequency single-electron transistors (SETs). One of the expected properties of the ACDET concept is the ability of discriminating the number of photons in a light pulse. Photon number discrimination is an important feature for different quantum information protocols, which has up to now only been demonstrated in very few systems.

The development of the ACDET detector has been carried out due to its complexity within a collaboration funded by the European Union involving six partners with expertise in the fields of semiconductor growth, semiconductor acoustics, single-electron transistors, and quantum communication. The role of the PDI in this project is the investigation of the photon-to-carrier conversion and acoustic transport processes. For that purpose, we have designed and fabricated the (Al,Ga)As layer structure of the detector and developed a prototype, where the transported charge is detected by n - and p -type doped regions. The electrical detection of ambipolar transport [P. D. Batista *et al.*, Appl. Phys. Lett. **93**, 262108 (2008)] as well as the use of metal guides to control the carrier flow required for the detector operation are new features that have not been addressed in previous investigations of ambipolar transport. We show that overall detection efficiencies (defined by the ratio of the number of electrically detected carriers and the number of incident photons) close to 60% can be achieved by using a microcavity structure to increase photon absorption. By taking into account that only 70% of the incoming photons are absorbed, we estimate acoustic transport efficiencies of about 85%, thus demonstrating the potential of acoustic transport for applications. In a subsequent step, SETs will be added to these structures in order to achieve single-charge sensitivity.

The studies of transport and manipulation of spins using the piezoelectric field of SAWs have been continued during this year with investigations of spin transport in quantum wells

(QWs) with (100) and (110) orientations. In both cases, the spins are generated by photoabsorption of circularly polarized light and detected by analyzing the polarization of the photoluminescence due to the recombination of the transported carriers. In case of (100) QWs, we have investigated processes to improve the spin transport efficiency using dynamic dots by optimizing the spin photo-excitation process and the subsequent recombination.

The activities on (110) quantum wells are motivated by the long lifetimes for spins oriented along the growth direction in these structures, which arise from a symmetry-related suppression of the D'yakonov-Perel' spin scattering mechanism. These studies are aimed at the transport of optically generated spins up to liquid nitrogen temperatures and carried out in the framework of an external project supported by the DFG. An important result was the demonstration that spins oriented along the growth direction can be transported over distances exceeding $60 \mu\text{m}$ up to at least liquid nitrogen temperatures. It has also been shown that the lateral carrier confinement during transport plays an important role in the suppression of spin-scattering mechanisms. In order to increase the photon-to-carrier conversion process, the (110) GaAs QW used as a transport channel is embedded in an (Al,Ga)As microcavity. Spin transport and manipulation in this kind of structures has been demonstrated at 80 K.

Finally, we address a new research area devoted to the control of microcavity polaritons (MCPs) using non-piezoelectric acoustic fields. MCPs are presently receiving considerable attention due to interesting properties such as low-threshold lasing, optical nonlinearities, optical parametric oscillation, and bosonic many-body interactions (Bose-Einstein condensation and superfluidity). The exploitation of these properties requires processes to control and manipulate these uncharged particles without destabilizing them. The use of the band-gap modulation by strain fields represents a promising option. Previously, we have demonstrated the modulation of MCPs using conventional SAWs propagating along a $\langle 110 \rangle$ direction of (100) (Al,Ga)As microcavities. A serious limitation of this approach results from the exciton dissociation by the SAW longitudinal piezoelectric field, which limits the MCP lifetime. This limitation is overcome by using SAWs propagating along a $\langle 100 \rangle$ direction of the (001) surface, which do not carry a longitudinal piezoelectric field. The generation of propagating non-piezoelectric modes in (Al,Ga)As microcavities with high quality factor is non-trivial and could only be achieved by reducing the thickness of the Bragg mirror as well as the Al content of the layers. Experiments on these structures show that the MCP modulation by SAWs can indeed be achieved without deteriorating the MCP linewidths. The latter is an important requirement for the observation of MCP-related Bosonic effects such as condensation and superfluidity.

2.2.1 Efficient transport of photogenerated electrons and holes in GaAs using surface acoustic waves: Application in single-photon detectors

Single-photon detectors (SPDs) are receiving substantial attention due to applications in a number of areas of applied physics such as low-light-level spectroscopy, optical sensors and quantum information processing. Different approaches have been proposed for the realization of solid-state SPDs including avalanche photodiodes, quantum dot transistors, and superconducting bolometers. Recently, we have proposed a novel concept for single-photon detection based on the combination of the transport of photogenerated electrons and holes by a surface acoustic wave (SAW) with charge detection by single electron transistors (SETs) [V. I. Talyanskii *et al.*, *Semicond. Sci. Technol.* **22**, 209 (2007)]. A schematic diagram of the detector is illustrated in Fig. 11(a). The incoming photons generate electrons and holes within the photon

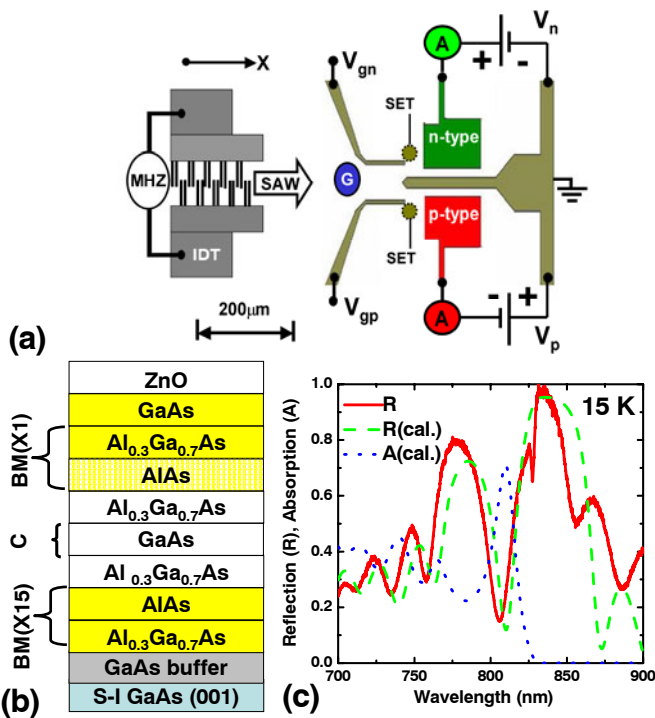


Fig. 11. (a) Schematic view and (b) layer structure of the detector grown on a semi-insulating (SI) GaAs (100) substrate and (c) its measured reflectivity and calculated absorptivity. Electrons and holes photoexcited at G are transported by the SAW as shown in (a) in the channel in-between the metal guides (g_n and g_p) towards the charge detection areas, where they are detected by either SETs or by p - and n -type contacts.

The carriers are detected by measuring the currents I_n and I_p arriving at p - and n -type contacts [cf. Fig. 1(a)] using electrometers. In order to improve photon absorption, the active GaAs layer [denoted as C in Fig. 11(b)] is inserted into an optical microcavity with Bragg mirrors (BMs) designed for resonance at a wavelength of $\lambda_L = 805$ nm. The whole structure is coated with a piezoelectric ZnO film to enhance the amplitude of the SAW fields. Figure 11(c) displays measured and calculated reflectivities (R) as well as calculated absorptivity (A) at $T = 15$ K, which reaches approx. 71% at λ_L .

absorption area G, which lies within the propagation path of a SAW excited by an interdigital transducer (IDT). The electrons and holes are attracted to the biased gates g_n and g_p and then transported along the x -direction by the SAW piezoelectric field toward the charge detection area, where they can be detected with single-charge resolution by SETs. The combination of ambipolar acoustic charge transport (ACT) with electrical detection leads to an efficient photon detector, where the processes of photon absorption, charge transport, and detection can be independently optimized.

The previous concept requires high photon absorption and acoustic transport efficiencies. In this contribution, we investigate these properties using a detector prototype without SETs, where the

The electrical response of the detector prototype was investigated by biasing the n - and p -contacts with voltages $V_n = -V_p = 2$ V and detecting the currents I_n and I_p . Illumination at spot G was provided by an 805 nm pulsed laser with intensity I_L . Figure 12 displays the ratio I_i/I_L ($i = n$ or p) for different values of I_L (from 5 to 50 nW) as a function of the nominal radio-frequency (rf) power P_{rf} applied to the IDT. The open and solid symbols show results for guide voltages $V_{gn} = -V_{gp} = 0$ and 0.5 V, respectively. Note that in all cases $I_n = -I_p$ as expected from the generation of the same number of electrons and holes by the incoming photons. The right vertical scale displays the total photon collection efficiency η of the detector, defined as the ratio between the number of detected electron-hole pairs ($N_{e,h}$) and the number of incident photons flux ($N_{e,h}^c$) according to

$$\eta = \frac{N_{e,h}^c}{N_{\text{ph}}} = \frac{\hbar\omega_L I_{p(n)}}{e I_L}, \quad (11)$$

where $\hbar\omega_L$ denotes the photon energy.

The acoustic fields are very weak for $P_{\text{rf}} < -10$ dBm. The current for $V_{gn} = -V_{gp} = 0$ V results from the collection of carriers that diffuse to the contacts. The effects of the SAW becomes apparent for $P_{\text{rf}} > 0$ dBm, when the piezoelectric field becomes sufficiently strong, ionizes the photoexcited excitons, and transports the free carriers to the contacts. The application of a guide voltage ($V_{gn} = -V_{gp} = 0.5$ V) promotes the separation of the photo-generated carriers, thus preventing recombination and increasing the collection efficiency η .

By taking into account the 71% absorptivity, the values of $\eta = 60\%$ recorded for low illumination levels ($I_L = 5$ nW) imply a transport and detection efficiency of approx. 85%, thus demonstrating that very few carriers are lost during transport and subsequent detection at the contacts. Note that the efficiency increases to values well above 100% for higher illumination intensities. This effect is attributed to an avalanche multiplication process at the reverse biased lateral pn -junction formed between the contacts.

In conclusion, the results on electrical detection of electrons and holes presented here demonstrate the efficient ambipolar acoustic transport over hundreds of μm , thus opening the way for the application of ambipolar SAW transport in high-sensitivity photon detectors.

(S. J. Jiao, P. D. Batista, R. Hey, P. V. Santos)

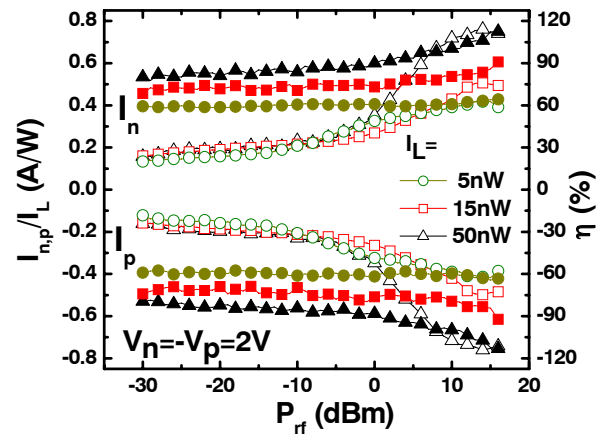


Fig. 12. Dependence of the currents I_n and I_p on the acoustic power P_{rf} applied to the IDT recorded under contact voltages $V_n = -V_p = 2$ V and guide voltages $V_{gn} = -V_{gp} = 0$ V (open symbols) and 0.5 V (solid symbols) [cf. Fig. 11(a)]. The right vertical scale shows the collection efficiency η [cf. Eq. (11)]. The experiments were carried out at 15 K with the laser spot G located $250 \mu\text{m}$ away from the contacts.

2.2.2 Spin relaxation during acoustic transport in (110) GaAs quantum wells

Considerable attention has been devoted to the control of the mechanisms limiting spin coherence in semiconductor systems because of the potential application of spins in quantum information processing. In this context, (110) GaAs quantum wells are promising candidates due to their long spin lifetimes. The long lifetime is a consequence of the suppression of the D'yakonov-Perel' (DP) relaxation mechanism for spins oriented along the growth direction $z \parallel [110]$. In addition to DP, other spin relaxation mechanisms such as the spin relaxation via exchange interaction between electrons and holes [the so-called Bir-Aronov-Pikus (BAP) mechanism] can also be very effective in reducing the spin lifetime of photogenerated carriers and need to be controlled.

In this contribution, we investigate the relevant spin relaxation mechanisms acting on z -oriented spins in intrinsic (110) GaAs QWs during the transport by surface acoustic waves (SAWs). SAWs with a wavelength of $\lambda_{\text{SAW}} = 5.6 \mu\text{m}$ were generated along the $x \parallel [001]$ direction of the QW plane using interdigital transducers (IDTs). Spin-polarized carriers were photogenerated along the transport path using circularly polarized light. The moving SAW piezoelectric potential Φ_{SAW} transports the carriers over distances exceeding $120 \mu\text{m}$, as indicated in the inset of Fig. 13(a). The right (I_R) and left (I_L) circularly polarized photoluminescence (PL) intensities emitted along the transport path was measured and used to determine the degree of spin polarization $\rho_z = (I_R - I_L)/(I_R + I_L)$.

The spin relaxation studies were carried out by measuring the spin transport lengths (ℓ_s) as a function of temperature, excitation light intensity, and acoustic power. Figure 13(a) shows ρ_z along the transport path for different temperatures (T). The ℓ_s values obtained from the decay of the spatial profiles are essentially independent of T up to at least 75 K. Higher temperatures could not be accessed due to the low carrier transport efficiency. The invariance of the spin lifetime with increasing temperature is in contrast to an increase reported in literature, where no SAW was applied. This invariance is attributed to the fact that the type-II spatial separation of carriers induced by Φ_{SAW} screens the electron-hole exchange interaction very efficiently, thus leading to long carrier as well as long spin lifetimes over the whole temperature range. The absence of BAP relaxation also accounts for the observed weak dependence of ρ_z on the light excitation intensity (not shown here).

We have found that the spin lifetime $\tau_z (= \ell_s/v_{\text{SAW}}$, where v_{SAW} denotes the SAW velocity) during transport depends sensitively on the SAW linear power density P_{SAW} , as indicated in Fig. 13(b). τ_z decreases with P_{SAW} for $P_{\text{SAW}} > 100 \text{ W/m}$ — this effect is investigated in detail in report 2.2.3. In contrast, τ_z increases from 12 to 22 ns for low powers ($5 \text{ W/m} < P_{\text{SAW}} < 92 \text{ W/m}$), thus demonstrating that the acoustic power can be used to tune the spin relaxation rate. τ_z in (110) QWs becomes limited by spin-orbit effects associated with the structural inversion asymmetry introduced, for instance, by asymmetric QW interfaces. The latter generates small in-plane effective magnetic fields, which rotate the z -oriented spins toward the QW plane, where

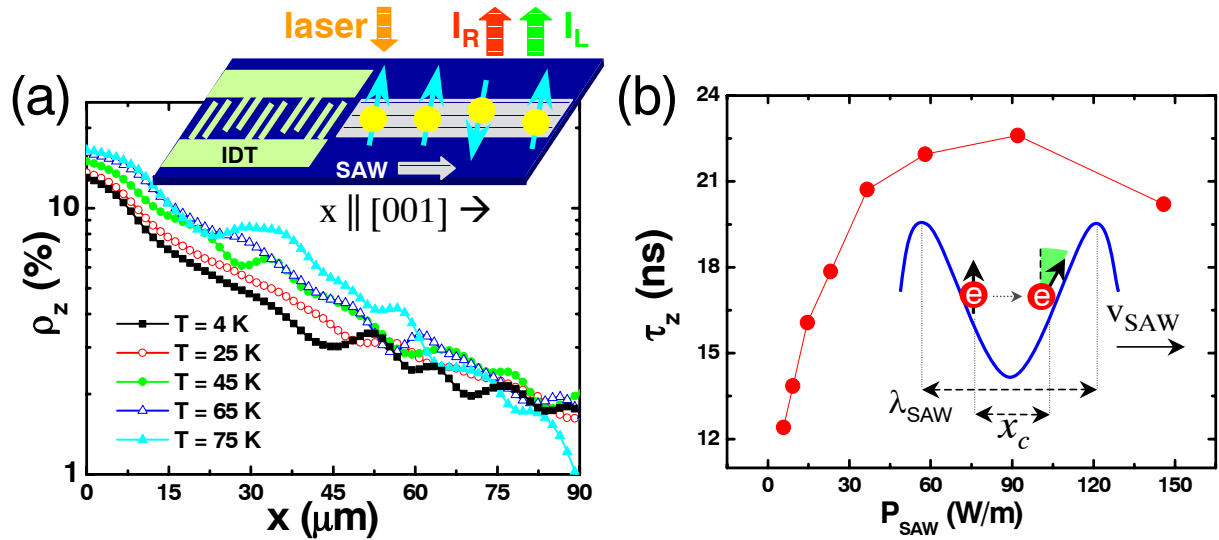


Fig. 13. (a) Spin polarization ρ_z along the transport path for different temperatures measured using the setup depicted in the inset. (b) Spin lifetimes τ_z as a function of P_{SAW} . Inset: electron confinement by the SAW field.

they become sensitive to DP relaxation. The enhancement of the spin lifetime with P_{SAW} is attributed to a progressive lateral confinement of the spins within submicrometer-wide potential wires oriented along the SAW wavefronts, as illustrated in the inset of Fig.13(b). Electron scattering at the potential boundaries makes the spin motion quasi-one-dimensional. Thus, the relaxation of in-plane spins is prevented via motional narrowing effects.

The effectiveness of the lateral confinement can be estimated from the ratio between the carrier confinement dimension (x_c) induced by the SAW piezoelectric potential and the spin-orbit length (λ_{SO}) associated with the in-plane spin component according to

$$\frac{x_c}{\lambda_{\text{SO}}} = \frac{\pi \gamma m_0 \lambda_{\text{SAW}}}{\hbar^2 d_{\text{eff}}^2} \sqrt{\frac{k_{\text{B}} T}{2\Phi_0}}. \quad (12)$$

Here, γ is the spin-orbit constant for GaAs, m_0 the electron effective mass, d_{eff} the effective QW thickness, and Φ_0 the amplitude of Φ_{SAW} . Even for low acoustic powers such as 5 W/m, numerical calculations yield $\Phi_0 = 60$ mV, which corresponds to $x_c/\lambda_{\text{SO}} \approx 0.07$ at $T = 15$ K. Therefore, the carriers are efficiently squeezed near the energy minimum of the acoustic potential, which moves slowly along the x direction with the velocity v_{SAW} . The fast thermal motion becomes essentially one-dimensional, thereby enhancing τ_z up to 22 ns, which corresponds to $\ell_s = 64 \mu\text{m}$.

In conclusion, the long spin lifetimes during acoustic transport in (110) QWs are attributed not only to the suppression of the electron-hole exchange, but also to the quasi-one-dimensional thermal spin motion induced by the type-II SAW piezoelectric field.

(O. D. D. Couto, Jr., K. Biermann, R. Hey, P. V. Santos)

2.2.3 Spin transport at liquid-nitrogen temperatures in GaAs-based microcavity structures

The specific symmetry of (110) GaAs quantum wells (QWs) prevents the dephasing via the D'yakonov-Perel' (DP) mechanism of electron spins optically aligned along the growth axis. When a surface acoustic wave (SAW) is generated on the surface of such a QW structure, the dynamic piezoelectric field of the SAW captures the optically generated electrons and holes at its potential maxima and minima, respectively, transporting these carriers with the acoustic velocity (v_{SAW}). The spatial separation reduces the exchange interaction of the spin-polarized electrons with the randomly polarized holes [Bir-Aronov-Pikus (BAP) spin-dephasing mechanism]. The combined suppression of the DP and BAP mechanisms leads to very long spin lifetimes and consequently long acoustic transport distances at low temperatures (15 K) [O. D. D. Couto *et al.*, Phys. Rev. Lett. **98**, 036603 (2007)].

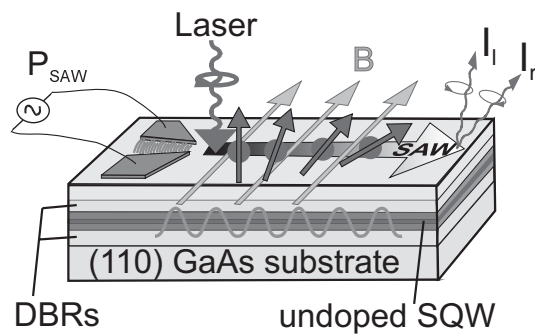


Fig. 14. Schematic diagram of the experimental configuration.

In this contribution, we investigate the spin transport by SAWs in an undoped (110) GaAs QW at 80 K, using the setup illustrated in Fig. 14. Circularly polarized laser light is focused onto a small generation spot with a diameter of about $4 \mu\text{m}$. The out-of-plane spin-polarized carriers generated in the undoped GaAs QW are then transported along the [001] direction by the SAWs ($\lambda_{\text{SAW}} = 5.6 \mu\text{m}$). The fixed propagation velocity of the SAWs of $v_{\text{SAW}} = 3.03 \mu\text{m/ns}$ provides a well-defined distance versus time relationship. Finally, we use spatially resolved measurements of the right (I_R) and left (I_L) circularly polarized photoluminescence (PL) intensities to determine the electron spin polarization ρ_z defined by $\rho_z = (I_R - I_L)/(I_R + I_L)$.

To determine the electron spin dephasing dynamics, a reasonable intensity of the PL signal away from the generation point is indispensable. However, increasing the temperature from 15 to 80 K decreases the PL efficiency of the QW considerably. It is not possible to compensate for the reduced PL efficiency by increasing the excitation density, as the density of photo-generated carriers that can be transported by the SAWs becomes limited by the carrier induced screening of the piezoelectric field. In order to enhance the PL efficiency and thus to observe the spin transport at $T = 80 \text{ K}$, the undoped 20-nm-thick QW is embedded between two distributed Bragg reflectors (DBRs). The $3.4\text{-}\mu\text{m}$ -thick microcavity structure was grown on a semi-insulating (110) GaAs substrate by molecular beam epitaxy at a relatively low temperature ($T_g = 490 \text{ }^\circ\text{C}$) and at a high V/III beam equivalent pressure ratio of 45 in order to avoid the faceting effects during growth. Furthermore, all the ternary layers of the structure consist of short-period superlattices to reduce the defect density as well as to circumvent strain relaxation due to the reduced critical thickness of (Al,Ga)As alloys on (110) substrates.

The symmetry of (110) QWs suppresses the dephasing via the DP mechanism of the out-of-plane (i. e., along z) polarized spins. However, any magnetic field not aligned along the z direction will rotate the spin polarization vector (as sketched in Fig. 14) creating an in-plane spin component. As the latter is subject to the DP dephasing mechanism, its spin lifetime is expected to be much shorter than the one of the z component, resulting in anisotropic spin dephasing. In addition to an applied external magnetic field (B_{ext}), the internal effective magnetic field induced by the SAW fields (B_{SAW}) can be utilized to rotate the spin polarization vector. B_{SAW} originates from the piezoelectric field of the SAW and can be described as Bychkov-Rashba field (B_{BR}). A second contribution to B_{SAW} is due to the SAW's shear strain component s_{xz} (B_{strain}). In the case of electron transport along $x \parallel [001]$, both contributions are aligned along $y \parallel [1\bar{1}0]$ and add up to an effective SAW-inherent magnetic field $B_{\text{SAW}} = B_{\text{BR}} + B_{\text{strain}}$. In our experiment, B_{SAW} is aligned in the same direction as B_{ext} (cf. Fig. 14).

Figure 15(a) illustrates spin transport with negligible spin vector rotation, i. e., using only weak SAWs ($P_{\text{SAW}} = 30 \text{ W/m}$) and without applying an external magnetic field. The data points depict the spin polarization as a function of transport distance, with the generation point set to $x = 0$. The solid line represents the best fit to an anisotropic spin-dephasing model yielding a transport length of $24 \mu\text{m}$ and a corresponding spin dephasing time of the out-of-plane component of 8.1 ns . The spin lifetime reduces significantly when either B_{SAW} is raised by strongly increasing P_{SAW} (187 W/m) or when an external magnetic field of $B_{\text{ext}} = 40 \text{ mT}$ is applied, as depicted in Fig. 15(b). Based on these measurements, the short spin dephasing time of the in-plane component can be estimated to be below 1 ns . In order to confirm the short in-plane spin lifetime, Hanle effect measurements were carried out in the spin diffusion configuration (not shown), which yield a consistent in-plane spin lifetime of 0.7 ns , thus confirming the strongly anisotropic spin dephasing behavior of (110) QWs.

Making use of the enhanced carrier-photon conversion in a microcavity structure, we were able to observe efficient spin transport in an undoped (110) GaAs QW at 80 K . We are planning to extend this concept toward room temperature.

(K. Biermann, O. D. D. Couto, Jr., R. Hey, P. V. Santos)

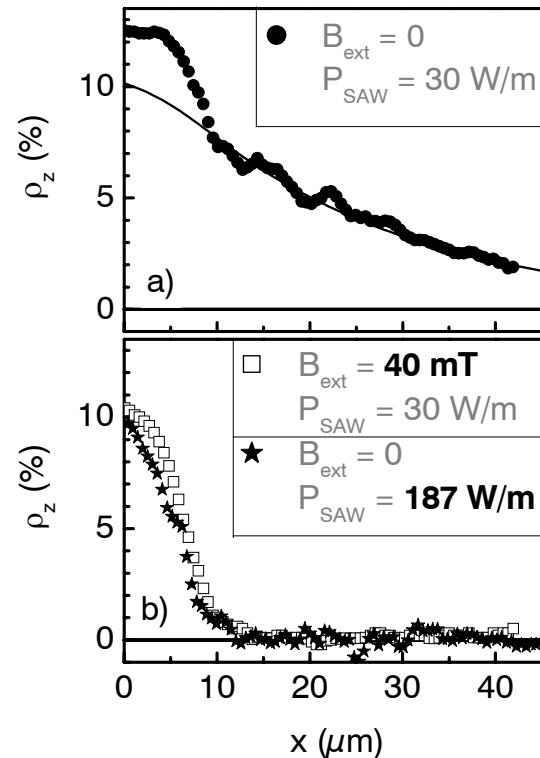


Fig. 15. Spin polarization ρ_z at $T = 80 \text{ K}$ as a function of transport length along $x \parallel [001]$ (a) with negligible and (b) with efficient spin polarization vector rotation.

2.2.4 Tunable polaritonic crystals formed by surface acoustic waves

Polaritons are quasi-particles resulting from the strong coupling between an exciton and a photon in a semiconductor. Two-dimensional or microcavity polaritons (MCPs) are formed when a quantum well (QW) is placed in an optical microcavity so that the wavefunctions of the confined excitons and photon modes overlap. Recently, lasing, optical nonlinearities, optical parametric oscillation, as well as bosonic many-body interactions such as Bose-Einstein condensation (BEC) and superfluidity have been intensely studied in MCPs. The exploitation of these interesting properties require processes to control and manipulate MCPs without destabilizing them. In a previous study [M. M. de Lima *et al.*, Phys. Rev Lett. **97**, 045501 (2006)], we have demonstrated the modulation of MCPs by electrically generated surface acoustic waves (SAWs) propagating along a $\langle 110 \rangle$ direction of (100) (Al,Ga)As structures. However, the modulation levels decrease at strong acoustic fields due to excitonic dissociation by the SAW longitudinal piezoelectric field.

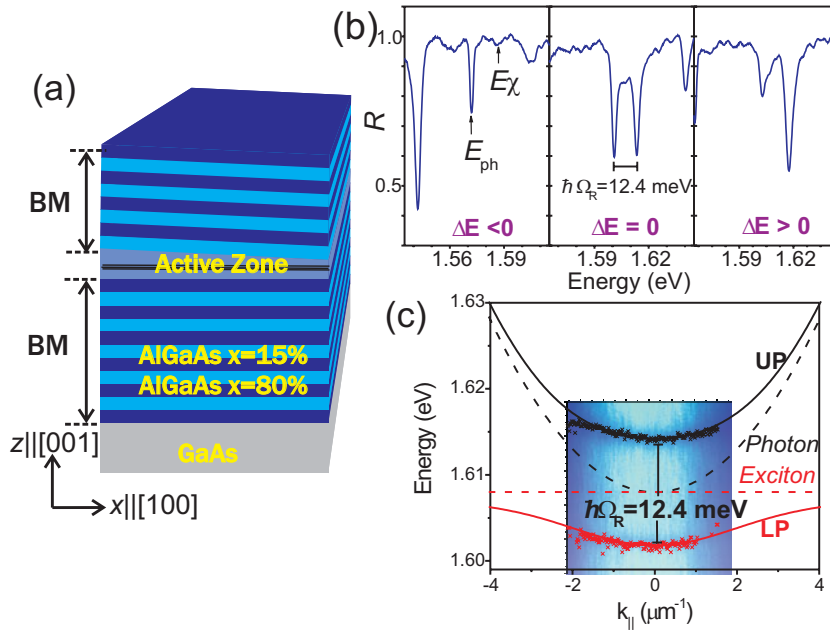


Fig. 16. (a) Schematic diagram of the MCP sample. The tapering of the cavity C allows the fine tuning of the optical resonance. (b) Reflectivity measurements for different detuning energies ΔE , yielding a Rabi splitting $\hbar\Omega_R = 12.4$ meV. (c) Measurement (image and crosses) versus fit (solid lines) of the dispersion of the upper (UP) and lower (LP) polariton branches. The dashed lines represent the uncoupled photon (parabolic) and the exciton (flat) dispersions.

The active zone of the MCP samples, which is based on designs reported in the literature, consists of a $\lambda/2$ cavity with 3 groups of 4 QWs located in regions of strong confinement of the electromagnetic field, i. e., at the center of the cavity and at the interfaces with the adjacent distributed Bragg mirrors (BMs). The large number of QWs enhances the exciton-photon coupling or Rabi-splitting ($\hbar\Omega_R$), which in our case is 12.4 meV. A tapering of the cavity as shown in Fig. 16(a) allows for the access of different detuning energies $\Delta E = E_\chi - E_{ph}$, where E_χ and E_{ph} are the bare exciton and cavity resonance energies [Fig. 16(b)]. The measured

In order to overcome this limitation, we present here an alternative approach based on the use of *non-piezoelectric* SAWs propagating along a $\langle 100 \rangle$ surface direction, which lacks this electric field component. These studies are expected to lead to novel applications such as compact and tunable optical devices for data processing and light modulation as well as optical-quantum encoding of information based on BEC in MCPs.

and calculated dispersion of the upper (UP) and lower (LP) polariton branches are shown in Fig. 16(c).

The generation of SAWs by interdigital transducers (IDT) along the non-piezoelectric [100]-direction was achieved by depositing a thin (600 nm thick) piezoelectric ZnO layer underneath the IDTs. In addition, the design of the BMs has to take into account the following requirements. First, the confinement of the acoustic energy at the surface relies on a waveguide effect induced by the lower acoustic velocity at the surface than in the bulk. Since the velocity in $\text{Al}_x\text{Ga}_{1-x}\text{As}$ alloys increases with composition x , the average Al composition of the BM has to be kept low ($x < 0.5$) to ensure the existence of SAW modes. Second, the cavity has to be placed within the decay length of the SAW field from the surface, which is approximately $\lambda_{\text{SAW}}/3$ with λ_{SAW} denoting the SAW wavelength. Finally, the strain-induced modulation of the excitonic energy has to be of type-I and in phase with the one of the microcavity resonance. These constraints limit the reflectivity of the top BM and, therefore, the Q -factor of the structure. A compromise was found by using 12 stacks for the upper BM in a MCP sample for $\lambda_{\text{SAW}} = 5.6 \mu\text{m}$, leading to a Q -factor of 1300.

The propagation of a SAW modulates the photon cavity and the excitonic energy producing a lateral, crystal-like potential for the MCPs with period λ_{SAW} . The effects of this modulation were studied by normal incidence reflectivity measurements at 15 K. Figure 17 displays the reflectivity profiles recorded as a function of the acoustic linear density P_{rf} , defined as the acoustic power divided by the lateral width of the SAW beam. The lateral modulation of the excitonic and photonic resonances splits both the LP and UP reflectivity dips, reaching values of up to 6 meV for $P_{\text{rf}} = 100 \text{ W/m}$. The observation of the splitting for both branches indicates that the non-piezoelectric acoustic field does not dissociate excitons, in contrast to the observation for piezoelectric SAWs.

In conclusion, we have demonstrated the effective modulation of MCPs by SAWs propagating in a non-piezoelectric direction. Samples with narrower linewidths (down to 0.6 meV), where the longer MCP coherence time will allow for the study of many-body phenomena, are currently under investigation. Furthermore, the interference of orthogonal SAWs provides zero-dimensional potentials to create potential dots with a high density of MCPs, which may be important for the observation of BEC.

(E. Cerda-Méndez, K. Biermann, R. Hey, P. V. Santos)

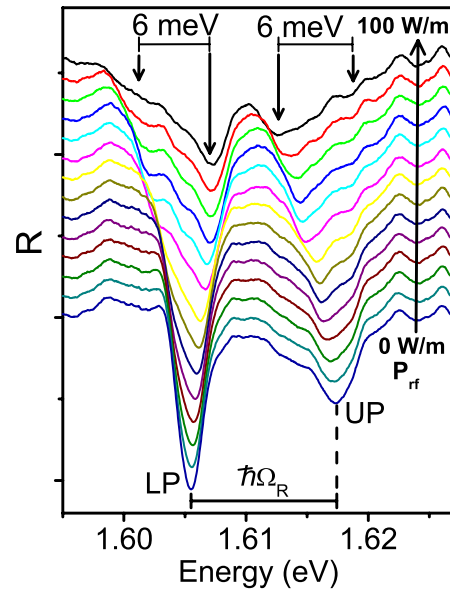


Fig. 17. Reflectivity (R) spectra of MCPs for a detuning energy $\Delta E = -6 \text{ meV}$ and increasing acoustic powers P_{rf} .